Validation of a Novel Methodology to Evaluate Changes in the Flare Geometry of Renovisceral Bridging Stent-Grafts After Fenestrated Endovascular Aneurysm Repair

Overeem, Simon; Schuurmann, Richte; Schumacher, Michiel; Jolink, Floortje; Ketel, Mirte; Nijendijk, Bob; Slump, Kees; Versluis, Michel; de Vries, Jean-Paul

Published in:
Journal of Endovascular Therapy

DOI:
10.1177/1526602820915932

Clinical Investigation

JOURNAL OF ENDOVASCULAR THERAPY
A SAGE Publication
An official publication of the ISEVS

Journal of Endovascular Therapy
2020, Vol. 27(3) 436–444

DOI: 10.1177/1526602820915932
www.jevt.org
SAGE

Validation of a Novel Methodology to Evaluate Changes in the Flare Geometry of Renovisceral Bridging Stent-Grafts After Fenestrated Endovascular Aneurysm Repair

Simon Overeem, PhD[1,2], Richte Schuurmann, PhD[2,3], Michiel Schumacher[1], Floortje Jolink[1], Mirte Ketel, MSc[1], Bob Nijendijk[1], Kees Slump, PhD[4], Michel Versluis, PhD[5], and Jean-Paul de Vries, MD, PhD[3]

Abstract

Purpose: To validate a novel method to evaluate changes in the geometry of renovisceral bridging stent-grafts (BSGs) in patients undergoing fenestrated endovascular aneurysm repair (fEVAR). **Materials and Methods:** Retrospective analysis was conducted of serial computed tomography angiograms (CTAs) of 10 fEVAR patients (31 BSGs) with at least 2 years of CTA follow-up. Centerline reconstructions were made through the fenestrated stent-graft (FSG) and each BSG. Flare geometry was reconstructed based on marker coordinates and a mesh of the aortic lumen. The shortest distance was calculated from the top of the flare circumference to the FSG fabric. The amount of flaring was assessed with the flare to fenestration diameter ratio and BSG compression to diameter ratio (D-ratio). All measurements were performed by 2 observers. Interobserver variability was assessed; results are presented as the intraclass correlation coefficient (ICC) and repeatability coefficient (RC). **Results:** Excellent interobserver agreement was achieved for BSG diameter and flare to fenestration distance calculations (ICC 0.865 and 0.944; RC 2.2% and 4.5%, respectively). Six patients had BSG-related complications during follow-up: 2 type IIIc endoleaks and 4 BSG occlusions. Five of the 6 BSGs with complications showed a considerable change in the D-ratio compared with the first postoperative CTA. **Conclusion:** Precise assessment of the geometry of visceral BSGs in fEVAR is feasible with the presented method. Geometrical changes that may precede later complications can be detected, which could aid in localization of the origin, but a larger series of patients is necessary to define its true clinical merit.

Keywords

aortic aneurysm, bridging stent-graft, complications, covered stents, endoleak, fenestrated stent-graft, flare, geometry, renal artery, renovisceral vessels

Introduction

Fenestrated endovascular aneurysm repair (fEVAR) of abdominal aortic aneurysms provides seal in the suprarenal aorta while preserving blood flow to the visceral arteries. The fenestrated technique is associated with high primary procedure success (99%), low perioperative mortality (4.1%), and low intraoperative target vessel occlusion (0.6%).[1] However, within 3 to 5 years after the primary procedure, 11% to 44% of fEVAR patients undergo secondary interventions related to occlusion of the target vessels (5% to 15%) and endoleak (4% to 10%) related to bridging stent-grafts (BSGs).[1–4]

[1]Department of Vascular Surgery, St Antonius Hospital, Nieuwegein, the Netherlands
[2]Multimodality Medical Imaging Group, Technical Medical Centre, University of Twente, Enschede, the Netherlands
[3]Department of Surgery, Division of Vascular Surgery, University Medical Centre Groningen, the Netherlands
[4]Robotics and Mechatronics, Technical Medical Centre, University of Twente, Enschede, the Netherlands
[5]Physics of Fluids Group, Technical Medical Centre, University of Twente, Enschede, the Netherlands

Corresponding Author:
Simon Overeem, Multimodality Medical Imaging Group, Technical Medical Centre, University of Twente, Drienerlolaan 5, 7522 NB Enschede, the Netherlands.
Email: spovereem@gmail.com

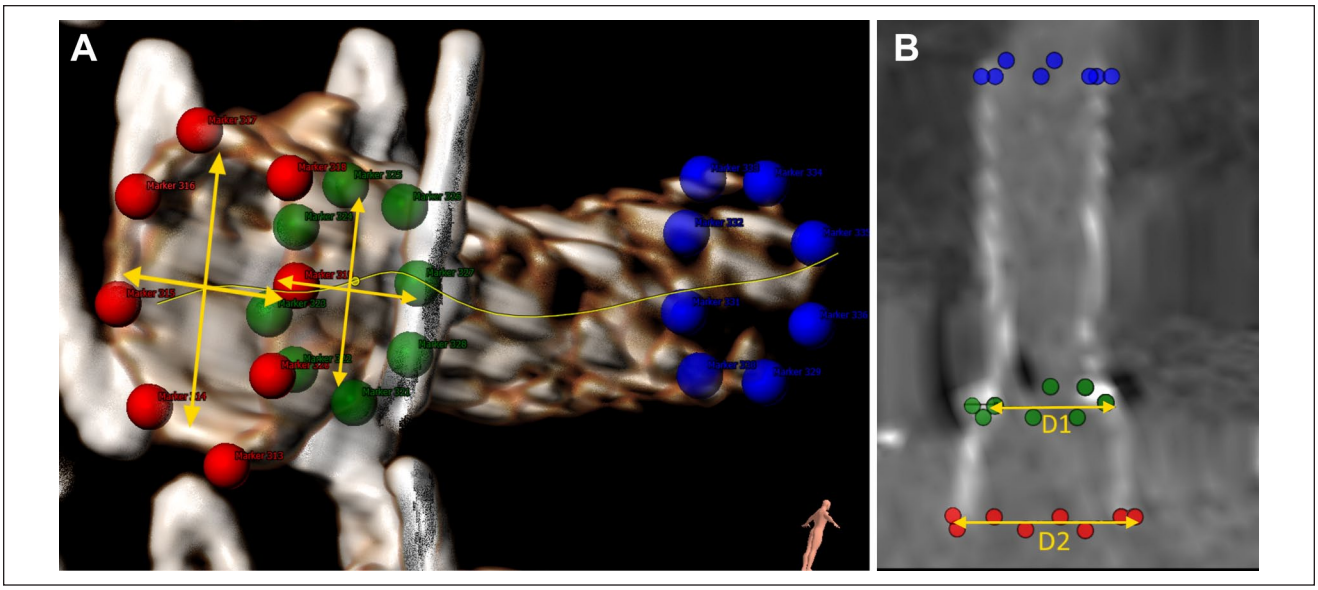

Figure 1. (A) Three-dimensional overview of the 8 red markers at the top of the flare, 8 green markers at the level of the fenestration, and 8 blue markers at the distal end of the bridging stent-graft (BSG). For the flare to fenestration ratio, minimum and maximum diameters were measured at the flare and at the level of the fenestration, indicated with the yellow arrows. (B) Stretched vessel view of the reconstructed image of the flaring of a celiac trunk BSG. Flare diameter (D2) and fenestration diameter (D1) are indicated.

BSGs are secured in the fenestrations of the main graft by flaring. Hemodynamic forces act on this connection, which can affect the position of the fenestrated stent-graft (FSG) and its BSG branches. This can result in compression or kinking of the BSGs in the target branches. Mismatch in diameter between the fenestration and the BSG and suboptimal flaring during the primary procedure may cause type IIIc endoleaks.[5] Moreover, a decrease in diameter of the flared end of the BSG could affect fixation and seal of the BSG in the fenestration, resulting in BSG displacement and endoleak during follow-up.

A study was conducted to validate a novel method of assessing BSG morphology, including the flared proximal segment, on post-fEVAR computed tomography angiography (CTA) scans.

Materials and Methods

Morphological Assessment

The postoperative geometry of FSGs and BSGs in the aorta and branch vessels was measured on a dedicated vascular workstation (3mensio Vascular, version 9.1; Bilthoven, the Netherlands) by 2 experienced observers (S.O. and B.N.). A main center lumen line (mCLL) was constructed semi-automatically in the mid flow lumen of the main endograft by manually positioning center points; the software used these points to automatically fit the mCLL. Separate BSG center lumen lines (bCLL) were constructed through the mid lumen of each stented branch artery in a similar manner with the branch vessel tool of the 3mensio workstation. A stretched vessel view was then constructed to allow measurement of centerline lengths and diameters perpendicular to the centerline. Minimum and maximum diameters of the BSGs were measured perpendicular to the bCLL, starting at the flare, in 1-mm intervals for the first 15 mm and then in 2-mm intervals over the length of the BSG.

The 3-dimensional (3D) orientation and geometry of the BSGs on the postoperative CTA scans were determined with 24 coordinate markers on the bCLL reconstructions. Eight markers were placed circumferentially at the top of the flare, 8 at the level of the fenestration, and 8 at the distal end of the BSGs (Figure 1A and B). The 3D coordinates of the mCLL, bCLLs, coordinate markers, and mesh of the aortic lumen and branch vessels were exported from 3mensio and loaded into dedicated software for automated geometrical analysis (MATLAB, 2017A; The MathWorks Inc, Natick, MA, USA).

The orientation and geometry of the BSGs were determined by 3 parameters specific to the devices.

Flare to Fabric Distance. The circumference of the flared edge of the BSG was determined by spline interpolation through the 8 coordinate markers. The distance was calculated for each of the 300 interpolated points over the circumference of the flare to the shadow projection point on

the mesh of the FSG fabric. The shadow projection points were calculated with the directional vector of the bCLL at the fenestration of the flare. The flare to fabric distance was calculated for each set of flare and shadow projection coordinates (Figure 2A). The flare to fabric distance was visualized in a color-scale over the 3D geometry of the flare (Figures 3–5).

Flare to Fenestration Diameter Ratio. The average diameter of the proximal flare edge (D2) was divided by the average diameter of the BSG at the level of the fenestration (D1) to obtain the flare to fenestration diameter ratio (Figure 2B). The flare to fenestration diameter ratio describes the amount of flaring of the BSG relative to the diameter at the fenestration.

BSG Compression Ratio (D-Ratio). The ratio of the major and minor axes of the BSG (D-ratio) was used to determine BSG compression (Figure 2C).[6] A D-ratio of 1 equals a circle, whereas higher values describe an oval shape and indicate BSG compression. Compression of the BSG was determined in 1- to 2-mm intervals over the entire length of the BSG. If >1 BSG was deployed within a branch artery, the total stented trajectory was assessed.

Patient Cohort and fEVAR Procedure

Validation of the method was performed on CTA scans of 10 patients (median age 81.5 years; 8 men) who underwent fEVAR for suprarenal AAA. All patients had significant comorbidities, including chronic pulmonary obstructive disease (n=4), coronary artery disease (n=3), chronic kidney disease (n=2), and congestive heart failure (n=2). The physical status of all patients was classified as American Society of Anesthesiologists class III. Median preoperative aneurysm size was 61.5 mm (interquartile range 58.5, 64.5).

All procedures were performed in a hybrid operating room using custom-made Zenith endografts (Cook Medical Inc, Bloomington, IN, USA). Advanta V12 stent-grafts (Getinge, Gothenburg, Sweden) were used as the BSGs in 9 patients, while the other patient received first-generation BeGrafts (Bentley Innomed, Hechingen, Germany). BSGs were oversized by 1 mm compared with the target vessel diameter. No nitinol extensions were deployed in these patients. The BSG flare was dilated with 12-×20-mm angioplasty balloons.

Post-fEVAR imaging consisted of an arterial phase CT scan with intravenous contrast (40–60 mL of Xenetix 350; Guerbet, Paris, France) and electrocardiographic gating at 70% of the RR interval during breath-hold. Tube voltage was 100 kV and slice thickness was 1.5 mm, with 0.75-mm spacing on a 256-slice CT scanner (Philips, Best, the Netherlands). Follow-up imaging was planned 30 days after fEVAR and annually thereafter.

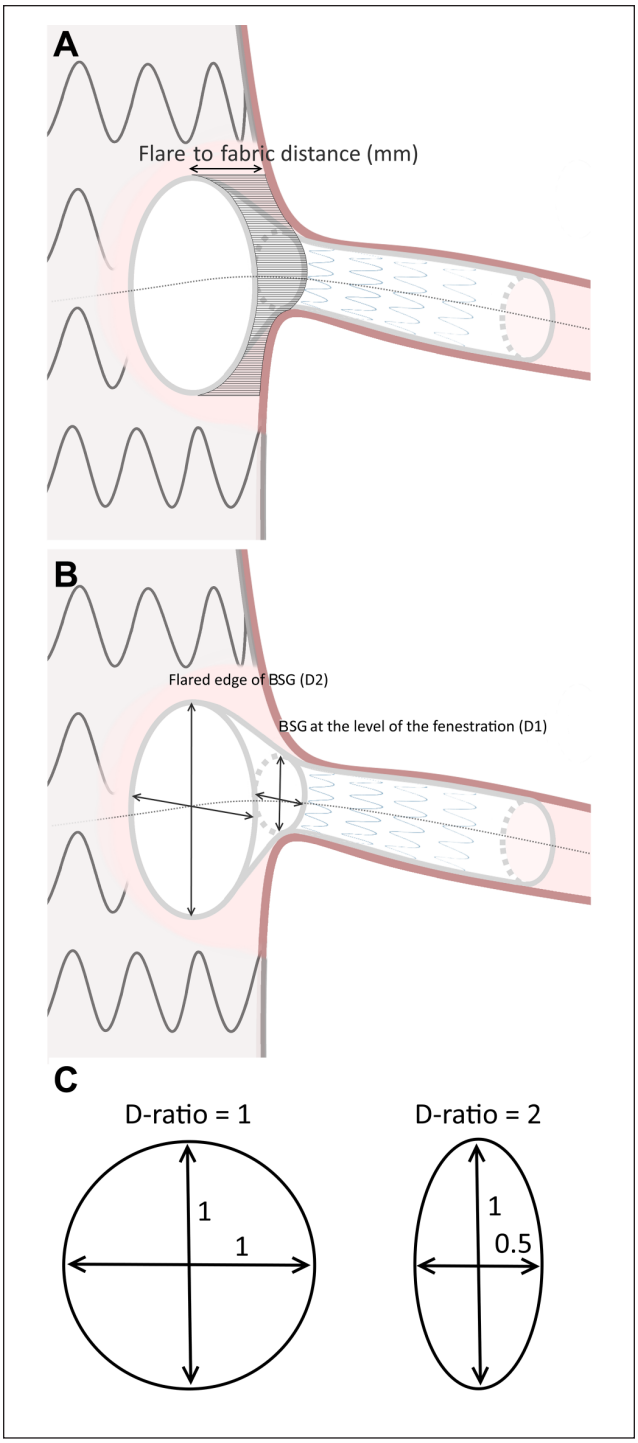

Figure 2. Schematic representation of the flare geometry. (A) The distance from the top of the flare to the fenestrated stent-graft (FSG) fabric (flare to fabric distance) is calculated for 300 consecutive points over the flare circumference. (B) The minimum and maximum diameters orthogonal to the bridging stent-graft (BSG) are measured at the flared top end (D2) and at the level of the fenestration (D1); they are used for the flare to fenestration diameter ratio. (C) The D-ratio was determined for the complete BSG trajectory. The D-ratio of the major and minor axes of a circle (left) and oval (right) are shown.

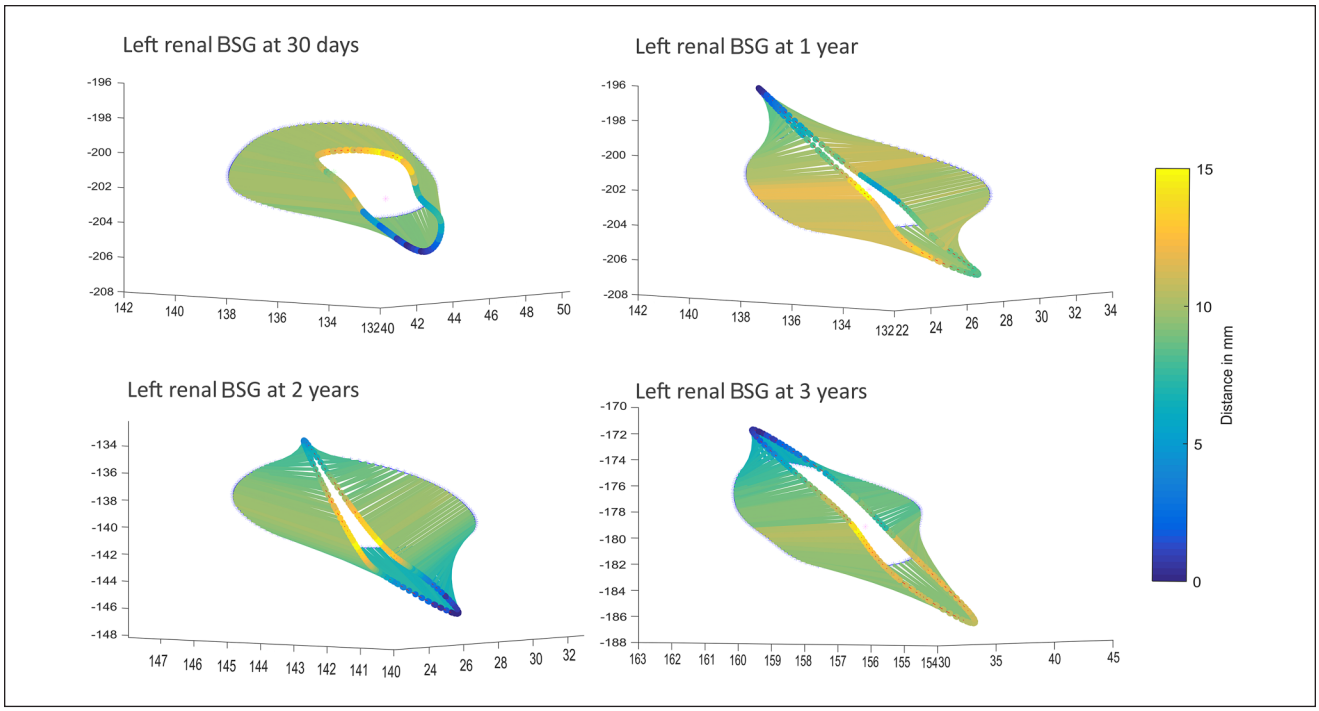

Figure 3. Left renal bridging stent-graft (BSG) over 3 years of follow-up. The flare was almost completely compressed at 1 year, resulting in stent occlusion at 3 years. No reintervention was planned. Axes are in millimeters.

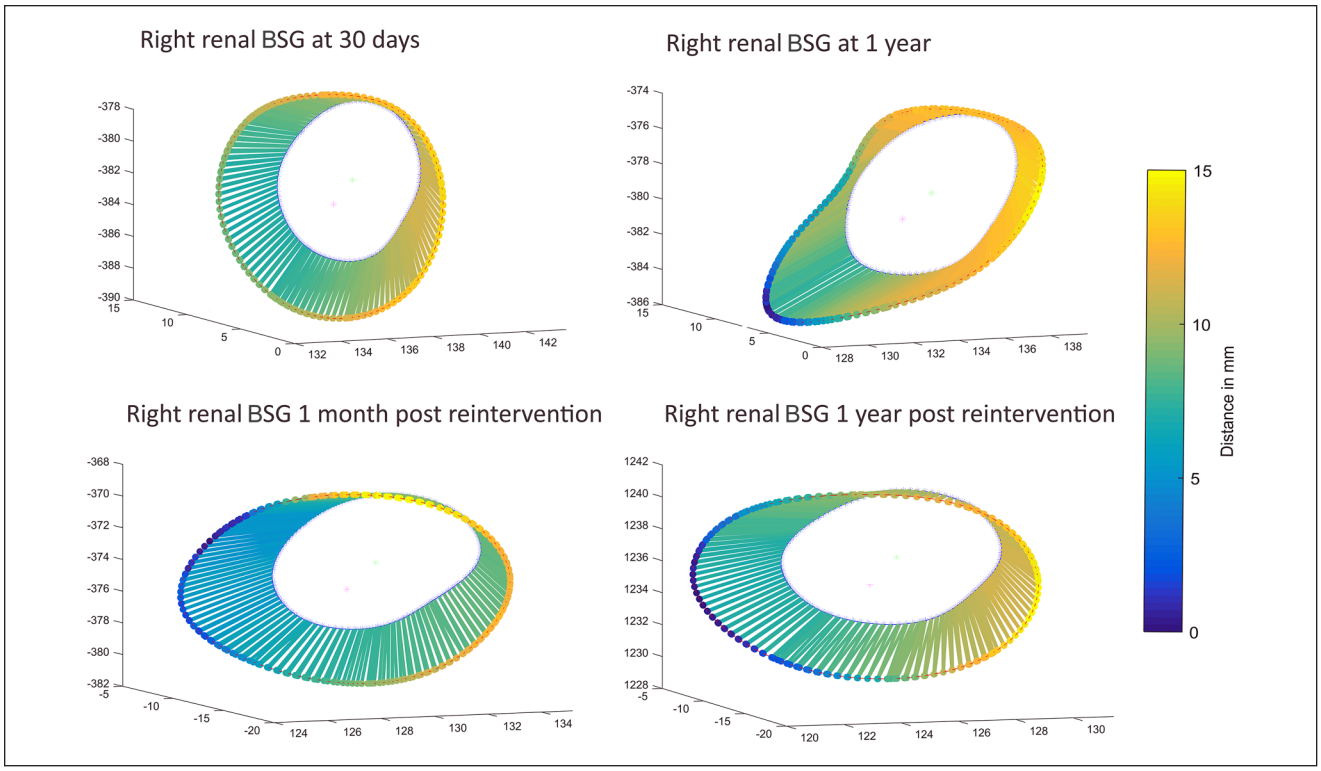

Figure 4. Right renal bridging stent-graft (BSG) over 2 years of follow-up. The reconstruction shows an oval shape of the flare at 1 year, resulting in type IIIc endoleak. Revision was performed 1 month later, and the endoleak was resolved. Axes are in millimeters.

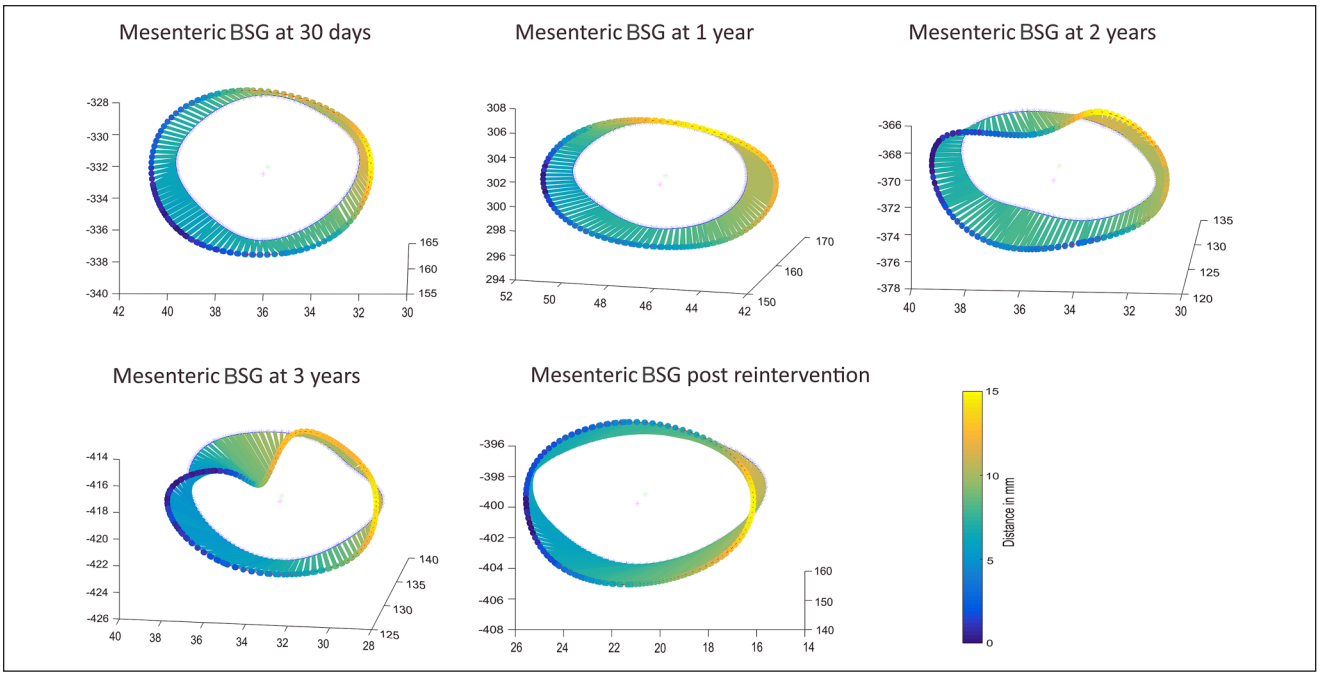

Figure 5. Superior mesenteric artery bridging stent-graft (BSG) evolution over 5 follow-up assessments. The reconstruction of the flare shows a dent in the flare at 2 years' follow-up, larger at 3 years, and leading to type IIIc endoleak. Revision surgery was performed 3.1 years after the primary intervention, and the endoleak was resolved. Axes are in millimeters.

Table 1. Bridging Stent-Graft (BSG)–Related Complications per Patient.

Patient	Complication	Follow-up	Reintervention
3	Occlusion of the right renal BSG	32 days	Thrombolysis
4	Occlusion of the left renal BSG	35 days	Thrombolysis
7	Type IIIc endoleak from the superior mesenteric artery BSG	3 years	Placement of a 7-×59-mm Advanta
8	Occlusion of the left renal BSG	3 years	Thrombolysis
9	Type IIIc endoleak from the right renal BSG	1 year	Placement of a 6-×38-mm Advanta
10	Stenosis at the fenestration for both renal BSGs. Occlusion of the left renal BSG at year 4.	3 years	None

Assessment of Complications

Complications associated with the BSG were defined as type IIIc endoleak and BSG stenosis or occlusion. Six patients with BSG-related complications were selected from the hospital's database of all fEVAR patients with these complications: 2 patients with type IIIc endoleak [one at the superior mesenteric artery (SMA) and the other at the right renal artery] and 4 patients with BSG occlusion (Table 1). No type Ia endoleak or stent-graft migration was observed in these patients. Three patients with occlusion underwent a secondary endovascular intervention. Four patients without complications at least 24 months after the procedure were selected as a reference. The study was approved by the hospital's review board and compliant with the Declaration of Helsinki. Informed consent was not required according to institutional policy on retrospective research.

Statistical Analysis

Continuous variables are expressed as mean ± standard deviation or median and interquartile range (IQR Q1, Q3). Interobserver agreements were determined for the flare to fabric distance and diameter measurements of 2 independent observers from the total of 31 BSGs. The 2 orthogonal diameters that were measured in 1- to 2-mm intervals over the bCLL were averaged, and the paired averages were compared between observers. Interobserver agreement was tested with the intraclass correlation coefficient (ICC), a 2-way mixed model by absolute agreement. ICC values >0.8 were considered to reflect good agreement. The mean difference of paired measurements was given as the repeatability coefficient (RC), which is defined as 1.96 times the standard deviation of the difference of paired observations. The RC describes the 95% confidence interval (CI) of the

measurement variability.[7] The Friedman test was used to compare changes in diameters over time, which were considered significant at $p<0.05$. Statistical analysis was performed with SPSS software (version 25; IBM Corporation, Armonk, NY, USA).

Results

Interobserver Agreement

Interobserver agreement for the BSG diameter measurements over the complete BSG trajectory was excellent (ICC 0.865, 95% CI 0.835 to 0.889), as was the agreement for the flare to fabric distance (ICC 0.944, 95% CI 0.940 to 0.947). The mean difference between measurements of BSG diameter was 0.03 mm with an RC of 1.55 mm. The mean difference between repeated measurements for the flare to fabric distance was 0.1 mm, with an RC of 1.65 mm.

Procedure Outcomes and Complications

A total of 31 BSGs were deployed (20 renal arteries, 7 SMA, and 4 celiac trunks). Three celiac scallops and 3 SMA scallops were not stented. Technical success (defined as successful completion of fEVAR with the FSG, patent BSGs, and no evidence for type I or III endoleak) was achieved in 9 patients. A BSG was not deployed in 1 patient because perioperative misalignment of the celiac trunk fenestration made it impossible to canalize the target artery. Exploratory diagnostic laparotomy because of abdominal pain did not show bowel ischemia.

Renal artery stenosis >50% was seen after 30 days in 2 patients on follow-up CTA. One underwent successful endovascular revision (Table 1); the other had unimpaired renal function (glomerular filtration rate ≥60 mL/min/1.73 m^2) and preferred no further treatment.

Over a median CTA follow-up of 33.7 months (minimum 23.1), 2 renal artery occlusions were observed at the 3-year CT follow-up. Both patients had shown reduced inferior pole contrast enhancement of the kidney on previous CT scans, but BSG stenosis was not reported. The 3-year patient underwent successful endovascular thrombolysis. Figure 3 shows the fenestration geometry of the occluded BSG at 3 years. With the new method, the left renal BSG showed increased compression of the flare (flare to fabric distance, flare to fenestration ratio, and D-ratio at the flared end changed from 9.7±0.3 mm, 1.1, and 1.4 at 30 days to 8.3±1.3 mm, 0.8, and 3.0 at 1 year, respectively). The BSG occluded at 3 years, but no reintervention was planned due to the patient's poor prognosis.

Late type IIIc endoleak developed in 2 patients. The endoleak in one was diagnosed 1 year after the primary intervention at the connection between the FSG and the BSG. The endoleak resolved after extending the BSG with a 6-×38-mm Advanta stent-graft and balloon molding the BSG (Figure 4). The mean flare to fabric distance, flare to fenestration ratio, and D-ratio at the flared end changed from 7.1±1.8 mm, 1.1, and 1.1 at 30 days to 8.4±0.9 mm, 1.3, and 1.5 at 1 year, respectively, so the flare cross-section became more oval. After reintervention, the 3 parameters at the flared end were 8.2±1.4 mm, 1.0, and 1.1.

The other patient, who had Marfan syndrome, had a type IIIc endoleak at the SMA fenestration, which was diagnosed 3 years after the primary intervention. Geometrical changes or suspicion of complications at this BSG were not mentioned in the reports of the radiologists on previous CT scans. The endoleak was successfully treated with a 7-×59-mm Advanta. The flare to fabric distance did not change over time, but the D-ratio at the flared end changed from 1.0 at 30 days to 1.1 at 1 year, 1.4 at 2 years, and 1.6 at 3 years; the flare cross-section became more oval with a dent (Figure 5). After reintervention at 3 years, the D-ratio at the flared end was again 1.0.

Geometry of BSGs

The flare to fabric distance, flare to fenestration diameter ratio, and D-ratio over time between the BSGs with vs without complications are summarized in Figure 6.

The average flare to fabric distance of all BSGs did not change significantly during follow-up: 6.9±2.5 mm, 6.6±2.4 mm, and 6.4±2.3 mm at 30 days, 1 year, and 2 years, respectively (p=0.894). The minimum and maximum flare to fabric distances also did not change significantly over time [maximum 8.7±2.7 mm, 8.6±3.0 mm, and 8.1±2.7 mm (p=0.801); minimum 5.5±3.0 mm, 5.1±3.0 mm, and 4.8±2.8 mm (p=0.942) at 30 days, 1 year, and 2 years, respectively.] However, some local changes of the flare to fabric distance were observed. Figure 7 shows an example of decreasing flare to fabric distance at the caudal site of a right renal BSG (5.6 mm, 4.4 mm, and 2.3 mm at 30 days, 1 year, and 2 years) as a result of BSG migration into the branch artery. Within the course of the study, no complication was observed in this BSG. Follow-up CTA was scheduled within 3 months.

For the flare to fenestration diameter ratio, the average diameter at the top of all renal BSG flares (n=20) did not change significantly (8.6±0.9 mm, 8.4±0.9 mm, and 8.4±1.0 mm, p=0.189), neither did the diameter at the level of the fenestration (7.0±1.2 mm, 6.8±1.0 mm, and 6.9±1.0 mm, p=0.905). The same trend was observed for the SMA and celiac trunk BSG flares. As a result, the mean flare to fenestration ratio of all BSGs did not change significantly during follow-up (1.2±0.2, 1.2±0.2, and 1.2±0.3, p=0.327). Eleven of 31 BSGs had >25% flaring, or >1.25 flare to fenestration ratio,

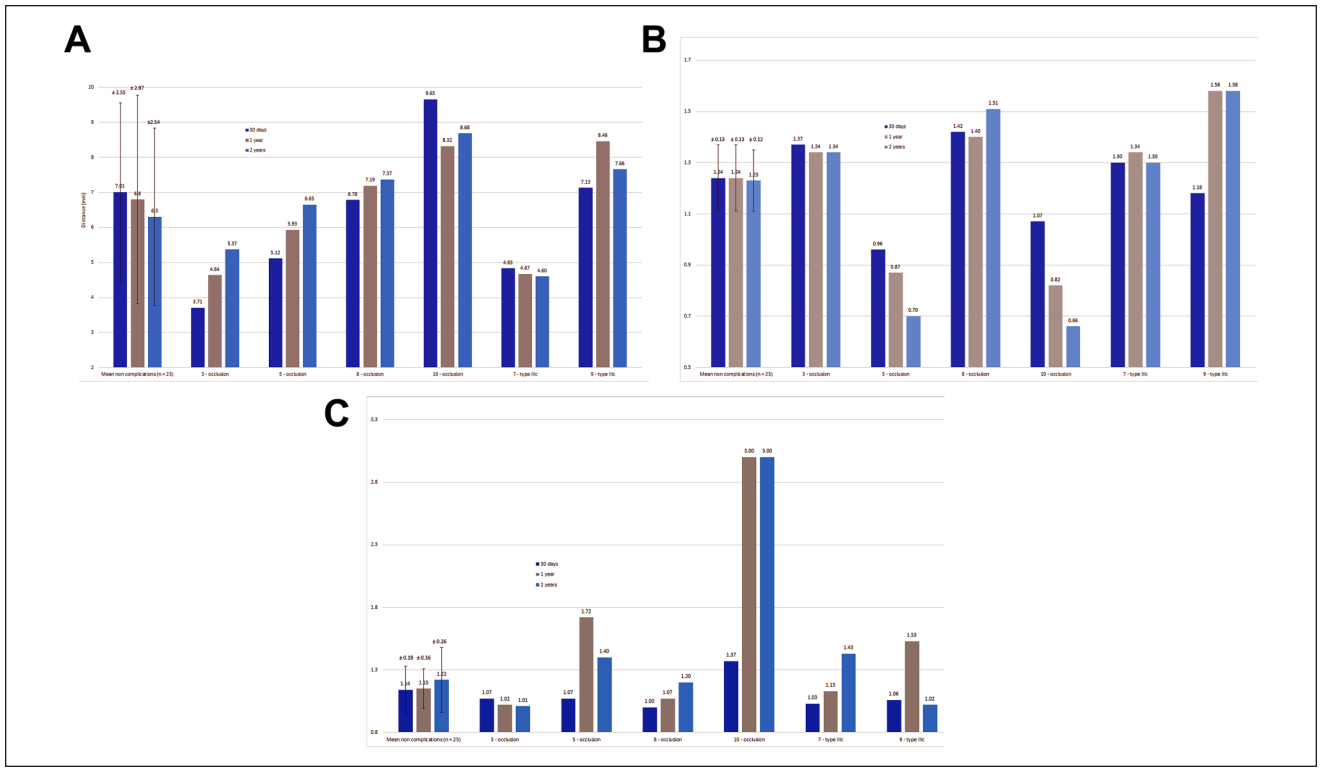

Figure 6. (A) Flare to fenestration diameter ratio, (B) flare to fabric distance, and (C) D-ratio for the no-complication group (n=25) vs the 6 BSGs with complications.

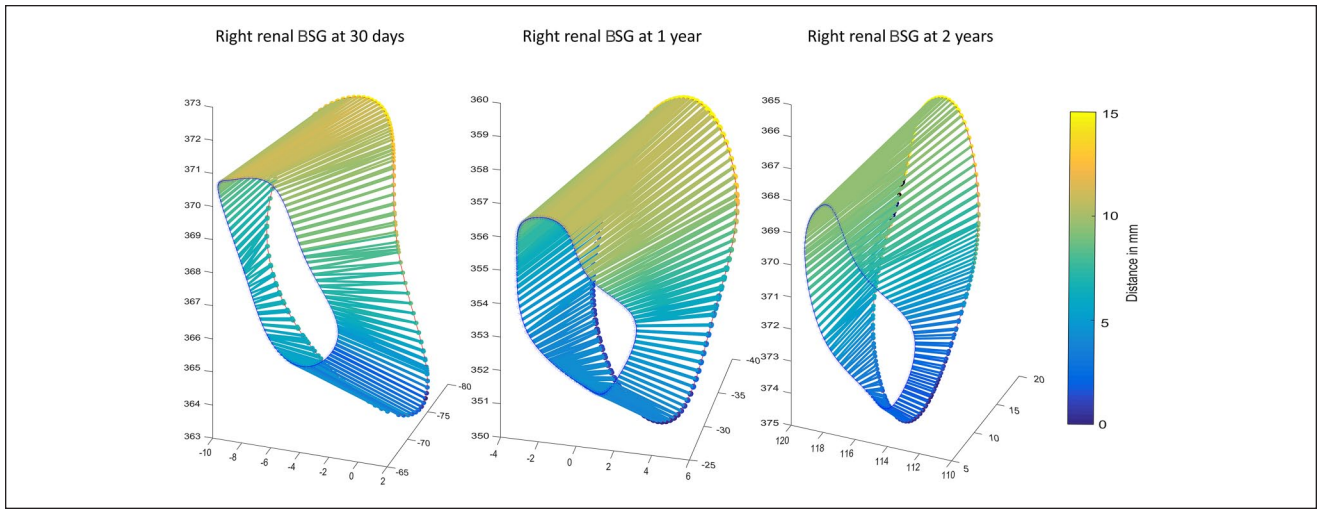

Figure 7. Flare to fabric distance of a right renal bridging stent-graft (BSG) over 2 years of follow-up. The decreasing flare to fabric distance at the caudal site suggests BSG migration into the branch artery.

whereas 5 BSGs had a <1.1 flare to fenestration ratio at 30 days. In the BSGs without complications, the mean flare to fenestration diameter ratio remained constant at 1.2±0.1, whereas the ratio changed considerably during follow-up in most patients with target vessel occlusion or type IIIc endoleak (Figure 6B).

The average D-ratio for all BSGs did not change significantly at 30 days, 1 year, and 2 years (1.1±0.2, 1.2±0.2, and 1.2±0.4, p=0.584). Contrary to the BSGs without complications, most BSGs with later complications showed a considerable change in the D-ratio compared with the first postoperative CTA (Figure 6C).

Discussion

This study introduces a semiautomated method for accurate analysis of the 3D geometry of BSGs. Geometrical analysis of consecutive post-fEVAR CT scans allows detection of subtle changes that may precede serious complications such as stent occlusion and type IIIc endoleak.

Most reinterventions after fEVAR are a result of type I or IIIc endoleak or loss of a target vessel.[3,4] Previous studies have shown angular changes of branching arteries after complex aneurysm repair.[8–11] The current study described BSG geometry in terms of distances and diameters of the flared part of the BSG and showed how this may be associated with complications after fEVAR. Besides suboptimal flaring, mismatch of BSG diameter with the branch artery or placement of a rigid stent in a tortuous vessel could also result in these complications. If a properly sized BSG is correctly dilated, there will probably be sufficient seal even without a flaring balloon.

Reproducibility of the flare to fabric distance and diameter measurements was excellent, and the variability of the measurements was similar to the variability of length and diameter measurements in the infrarenal neck for EVAR and fEVAR planning.[12–14] The geometrical parameters can be measured with high precision because the boundary of the metal stent frames is clearly delineated in the CTA scans.

Full compression of a BSG as assessed by the D-ratio results in occlusion of the branch, with devastating consequences to the end organ. Occlusion may be preceded by incremental increase in the compression of the BSG, sometimes resulting from FSG migration, which can be detected on the CT scans. BSG compression may also result in mismatch with the FSG, resulting in type IIIc endoleak. Accurate analysis of BSG compression on consecutive CT scans may therefore predict later complications, allowing timely reinterventions, and may aid in the correct classification of an endoleak. In the treatment of endoleaks after fEVAR, a correct assessment of the origin of the endoleak is crucial. Type Ia endoleak requires a different reintervention strategy than a type IIIc endoleak, and the software introduced here may aid in an accurate and precise determination of the origin of the endoleak. Five of the 6 BSGs with complications showed a significant increase of the flare to fenestration ratio or D-ratio.

Adequate flaring of the BSG is required to resist component displacement or migration and type IIIc endoleak. The amount of flaring and evolution of a decreased flare during follow-up can be determined by assessing the flare to fenestration diameter ratio on consecutive CT scans. There was a large variation in flare morphology of the assessed BSGs on the 30-day CT scan. Most BSGs were flared >25%, meaning that the BSG was 25% larger at the flared edge than at the level of the fenestration, but some BSGs were flared <10%, potentially affecting fixation of the BSG in the FSG. Both BSGs that developed a late type IIIc endoleak had <10% flare or decreased flare during follow-up.

As a result of hemodynamic forces and inadequate fixation of the BSG in the FSG, the BSG may displace or migrate into or out of the branch artery, as shown in Figure 7. The added value of the flare to fabric distance when one is comparing changes over time is the color-coded visualization of the circumference of the flare, emphasizing changes in geometry that may not be seen otherwise.

Limitations

The study was designed to validate a method for determining changes in geometry of BSGs in fEVAR patients, and the patients included in the study neither represented the average population of fEVAR patients nor were they consecutive or matched to patients without complications. The BSGs included in the study were not the same or equally distributed. The results of this study should therefore not be used as a reference to compare outcomes of different BSGs. In addition, the mean flare to fabric distance was not statistically different between BSGs with and without complications, and this did not change over time due to the small number of patients. A large clinical study with consecutive patients is required to determine the incidence of complications after fEVAR and the predictive value of accurate assessment of the BSG geometry.

The current method is based on accurate centerline reconstruction and placement of 3D coordinate markers. Although this could be done with high precision, measurements are time-consuming and possibly operator dependent. Future efforts in automatic segmentation of the FSG and branch BSGs should speed up the process and may further reduce interobserver variability. Although the diameter measurements were precise, with 95% of the paired measurements within 1.55 mm, this could still dramatically affect the flare to fenestration diameter ratios and D-ratios, since these diameters are only a few millimeters.

Migration of the FSG may result in component displacement, BSG occlusion, and type IIIc endoleak. Accurate determination of FSG displacement was not assessed,[15] which should be included in future studies with a larger consecutive patient cohort. Also, the dimensions of the fenestrations of the FSG were not available from the patient records. An oval fenestration could result in a different flaring pattern compared with a circular fenestration. This could not be verified in this study but is an interesting subject for future analysis.

BSG morphology may change during the cardiac cycle,[16,17] which may result in variable BSG orientation and D-ratios during the cycle. The CTA scans in this study were triggered at mid diastole, which should represent maximum compression,

but without dynamic imaging this could not be verified. Future research may focus on dynamic or multiphase CTA data to assess changes in BSG geometry during the cardiac cycle.

Conclusion

Accurate semiautomated assessment of BSG geometry can be performed with high precision using the method proposed in this study. Visualizing and quantifying the geometry of the individual BSG after fEVAR over time provides insight to potential modes of failure that may precede stent occlusion or type IIIc endoleak. Large variation was observed in BSG geometry in this small patient cohort. In all the BSGs with a type IIIc endoleak or occlusion, the complication was preceded by obvious change in the BSG geometry. A large consecutive patient series should determine the association between unfavorable BSG geometry and BSG-related complications and shed light on the true clinical value of this new method.

Declaration of Conflicting Interests

The author(s) declared no potential conflicts of interest with respect to the research, authorship, and/or publication of this article.

Funding

The author(s) received no financial support for the research, authorship, and/or publication of this article.

ORCID iD

Simon Overeem https://orcid.org/0000-0002-3282-6654

References

1. British Society for Endovascular Therapy and the Global Collaborators on Advanced Stent-Graft Techniques for Aneurysm Repair (GLOBALSTAR) Registry. Early results of fenestrated endovascular repair of juxtarenal aortic aneurysms in the United Kingdom. *Circulation*. 2012;125:2707–2715.
2. O'Callaghan A, Greenberg RK, Eagleton MJ, et al. Type Ia endoleaks after fenestrated and branched endografts may lead to component instability and increased aortic mortality. *J Vasc Surg*. 2015;61:908–914.
3. Roy I, Millen AM, Jones SM, et al. Long-term follow-up of fenestrated endovascular repair for juxtarenal aortic aneurysm. *Br J Surg*. 2017;104:1020–1027.
4. Kristmundsson T, Sonesson B, Dias N, et al. Outcomes of fenestrated endovascular repair of juxtarenal aortic aneurysm. *J Vasc Surg*. 2014;59:115–120.
5. Oderich GS. *Endovascular Aortic Repair. Current Techniques with Fenestrated, Branched and Parallel Stent-Grafts*. Cham Switzerland: Springer International; 2017. ISBN 978-3-319-15192-2
6. Overeem SP, Donselaar EJ, Reijnen MMPJ. In vitro quantification of gutter formation and chimney graft compression in chimney EVAR stent-graft configurations using electrocardiography-gated computed tomography. *J Endovasc Ther*. 2018;25:387–394.
7. British Standards Institution. *Precision of Test Methods I. Guide for the Determination and Reproducibility for a Standard Test Method*. London, England: British Standards Institution; 1979.
8. Ullery BW, Suh GY, Lee JT, et al. Geometry and respiratory-induced deformation of abdominal branch vessels and stents after complex endovascular aneurysm repair. *J Vasc Surg*. 2015;61:875–884.
9. Ullery BW, Suh G, Lee JT, et al. Comparative geometric analysis of renal artery anatomy before and after fenestrated or snorkel/chimney endovascular aneurysm repair. *J Vasc Surg*. 2016;63:922–929.
10. De Niet A, Post RB, Reijnen MMPJ. Geometric changes over time in bridging stents after branched and fenestrated endovascular repair for thoracoabdominal aneurysm. *J Vasc Surg*. 2019;770:702–709.
11. Suh G, Choi G, Herfkens RJ, et al. Respiration-induced deformations of the superior mesenteric and renal arteries in patients with abdominal aortic aneurysms. *J Vasc Interv Radiol*. 2013;24:1035–1042.
12. Ghatwary T, Karthikesalingam A, Patterson B, et al. St George's Vascular Institute Protocol: an accurate and reproducible methodology to enable comprehensive characterization of infrarenal abdominal aortic aneurysm morphology in clinical and research applications. *J Endovasc Ther*. 2012;19:400–414.
13. Banno H, Kobeiter H, Brossier J, et al. Inter-observer variability in sizing fenestrated and / or branched aortic stent-grafts. *Eur J Vasc Endovasc Surg*. 2013;47:45–52.
14. Oshin OA, England A, McWilliams RG, et al. Intra- and interobserver variability of target vessel measurement for fenestrated endovascular aneurysm repair. *J Endovasc Ther*. 2010;17:402–407.
15. Schuurmann RCL, Overeem SP, Ouriel K, et al. A semiautomated method for measuring the 3-dimensional fabric to renal artery distances to determine endograft position after endovascular aneurysm repair. *J Endovasc Ther*. 2017;24:5–15.
16. Draney MT, Zarins CK, Taylor CA. Three-dimensional analysis of renal artery bending motion during respiration. *J Endovasc Ther*. 2005;12:380–386.
17. Muhs BE, Vincken KL, Teutelink A, et al. Dynamic cine-computed tomography angiography imaging of standard and fenestrated endografts: differing effects on renal artery motion. *Vasc Endovascular Surg*. 2008;42:25–31.